ADVANCED OPTICAL MATERIALS
www.advopticalmat.de

Structural Modification Orientated Multifunctional AIE Fluorescence Probes: Organelles Imaging and Effective Photosensitizer for Photodynamic Therapy

Kongqi Chen, Rongyuan Zhang, Zhiming Wang, Weijie Zhang,* and Ben Zhong Tang**

Luminogens with aggregation-induced emission feature (AIEgens) are highly demanded because of its excellent performance in fluorescent bioprobes. In this work, three AIEgens based on tetraphenylethylene isoquinolinium (TPE-IQ) derivatives by introducing different electron donor and sterically hindered groups to replace the phenyl ring of the isoquinolinium core are prepared in a one-pot reaction with a high yield and characterized systematically. By the analysis of photophysical properties and theoretical calculations, the structure-property relationships among them become clear. Although they all inherit AIE feature as expected, these similar structural AIEgens present different organelle-targets, which is attributed to their different cellular uptake way and energy barrier to cell membrane by detailed experiments. In addition, these TPE-IQ-based AIEgens are potential candidates for photodynamic therapy originating from their activities of generating reactive oxygen species under visible light irradiation.

1. Introduction

Recently, fluorescent bioprobes have received increasing attention owing to their high spatial resolution, low cost, excellent selectivity, simple operation, and in situ workability,[1,2] which play a significate role in biological and medical fields. Of all applications, organelle imaging stands out because of its key role in supporting the normal functions of cells and the whole body.[3] In most cases, organelles of cells can reflect many information about health condition of body. For instance, mitochondria, known as the cellular power house, is related to many diseases and malfunctions in cellular aspects, such as cell malignancy, atherosclerosis, diabetes, and Alzheimer's disease.[4,5] And lysosome is involved in numerous key life activities including intracellular transportation, apoptosis, cholesterol homeostasis, and plasma membrane repair.[6,7] It is very clear that organelle disorder will cause a series of diseases and do harm to our health. However, conventional fluorescent bioprobes had suffered from some unavoidable drawbacks, such as low signal-noise ratio and poor photostability, mostly due to the troubling aggregation-caused quenching (ACQ) phenomenon.[8] For example, since the conventional fluorophores used as bioprobes can be so easily quenched in a high concentration that researchers have to utilize them in dilute solutions, leading to poor sensitivity and low resistance toward photobleaching,[9] which is a great impediment to their practical applications. By contrast, aggregation-induced emission luminogens (AIEgens), most of which possess a highly twisted conformation to achieve high solid-state quantum yield, have offered a straightforward solution to the ACQ problem.[10] Namely, the AIE fluorescent bioprobes can work at high concentrations and possess much better photostability,[9–11] facilitating the long-term tracking to some extent.[12]

Thus, the design of more AIE fluorescent bioprobes with specific organelle-targeting makes great difference, which not only enables us to follow the whole biological process in the living context by long-term tracking, but also can be used as potential therapeutic targets for disease treatment.[13–15] Recently, more attention has been paid to photodynamic therapy (PDT) because it can eliminate the malignant tumor cells with high specificity while not affecting normal cells, which is an advantage over chemotherapy.[16,17] The ability to specially target organelles and therefore real-time monitor their morphological changes, together with the effect of PDT treatment, will be highly important for fundamental and clinical research.[18] Fortunately, such fantastic characters had been achieved from

Dr. K. Chen, Prof. Z. Wang, Prof. B. Z. Tang
Center for Aggregation-Induced Emission
Key Laboratory of Luminescence from Molecular Aggregates of Guangdong Province
State Key Laboratory of Luminescent Materials and Devices
South China University of Technology
Guangzhou 510640, China
E-mail: wangzhiming@scut.edu.cn; tangbenz@ust.hk

Dr. R. Zhang, Dr. W. Zhang
Department of Urology
The First Affiliated Hospital of Soochow University
188 Shizi RD, Suzhou 215006, China
E-mail: wj539@163.com

Prof. Z. Wang, Dr. W. Zhang, Prof. B. Z. Tang
HKUST-Shenzhen Research Institute
Shenzhen 518057, China

Dr. W. Zhang, Prof. B. Z. Tang
Department of Chemistry
Hong Kong Branch of Chinese National Engineering Research Center for Tissue Restoration and Reconstruction
The Hong Kong University of Science and Technology
Clear Water Bay, Kowloon 999077, Hong Kong, China

The ORCID identification number(s) for the author(s) of this article can be found under https://doi.org/10.1002/adom.201901433.

DOI: 10.1002/adom.201901433

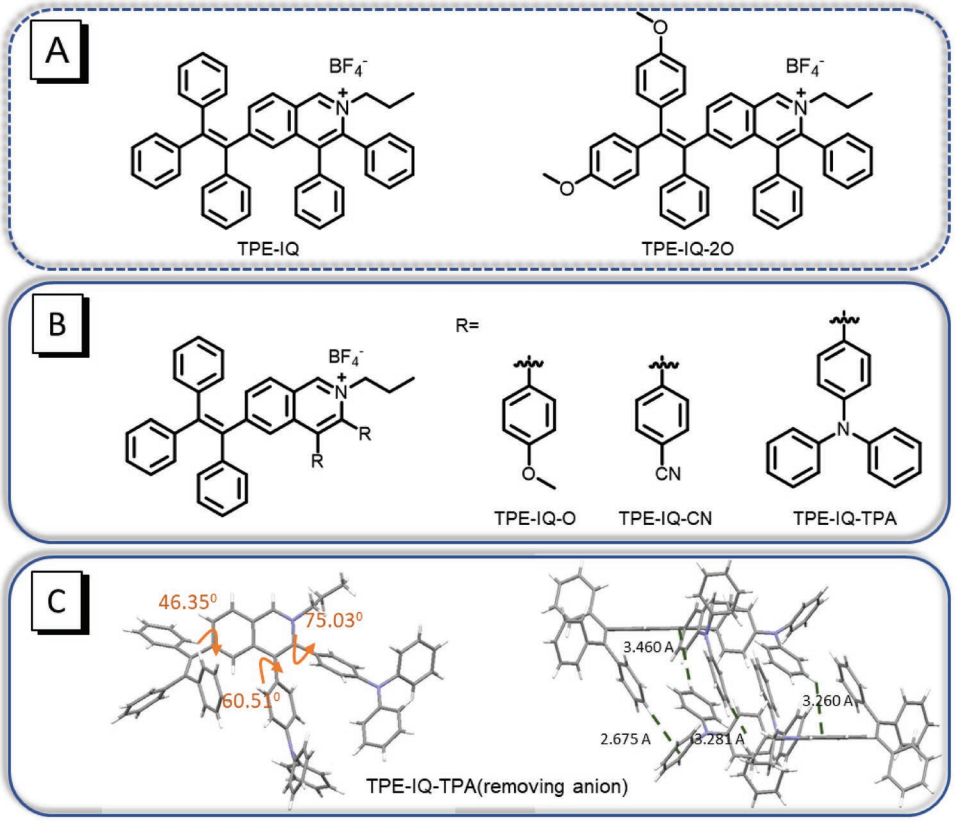

Scheme 1. A) Molecular structure of TPE-IQ and TPE-IQ-2O reported by our group before. B) Molecular structures of TPE-IQ-O, TPE-IQ-CN, and TPE-IQ-TPA; C) The crystal structure and stacking mode (intermolecular distance) of TPE-IQ-TPA removing the counter anion was obtained and shown in the ellipsoid style. Hydrogen, carbon, and nitrogen were shown in white, gray, and blue, respectively.

isoquinolinium (IQ)-based molecules with good target to mitochondria reported by our group before (**Scheme 1**).[19–21] However, the relationship between the difference of IQ-salts detailed structure and targeting-ability of them, especially their electrostaticity and spatial conformation tunings, is more important for the design of high-performance bioprobes.

Herein, three new tetraphenylethylene isoquinolinium (TPE-IQ)-based AIEgens, namely TPE-IQ-O, TPE-IQ-CN, and TPE-IQ-triphenylamine (TPA), had been successfully prepared and characterized by inserting different electron-donating/electron-withdrawing or sterically hindered groups to electron-deficient isoquinolinium core via simple reaction-substrate tunings (Scheme 1). As expected, they all exhibited AIE characteristic, and the different Zeta potentials of these TPE-IQ-based AIEgens were realized in aggregation. Interestingly, TPE-IQ-O could specially target mitochondria as like TPE-IQ and TPE-IQ-2O, while TPE-IQ-CN and TPE-IQ-TPA could target lysosome instead. More detail experiments were employed to account for their targeting difference, which might be caused by their different cellular uptake way and energy barrier to cell membrane. By the analysis of the MTT (3-(4,5-dimethylthiazol-2-yl)-2,5-diphenyltetrazolium bromide) experiment, we could find the dark cytotoxicity of three AIEgens showed great discrepancy because of their differences in targeting sites, but they all exhibited good killing capability to cancer cell under white light irradiation due to their reactive oxygen species (ROS) generation, implying these TPE-IQ-based AIEgens were potential photosensitizers for PDT process.

2. Results and Discussion

2.1. Synthesis and Crystal Structures

TPE-IQ-CN, TPE-IQ, TPE-IQ-O, and TPE-IQ-TPA (Scheme 1) were synthesized by condensation of corresponding aldehydes, diphenyl acetylene, and propylamine under the catalysis of $[RhCp^*Cl_2]_2$ and $AgBF_4$ with high yield of 65–80%. The synthesis processes and structural characterization using ESI-MS, ^1H NMR, and ^{13}C NMR are provided in the Supporting Information (Figures S1–S6, Supporting Information).

Unfortunately, the single crystals of these AIEgens with BF_4^- as anion were failed to obtain, but after anion exchange to BPh_4^-, only the TPE-IQ-TPA single crystal was obtained (Scheme 1). According to previous reports,[21] this packing mode of large π cations via anion substitution process had some certain reference significance for discussing its conformation distribution. As shown in **Figure 1**C, the isoquinolinium salt plane was set as a center, and the peripheral two TPA groups and triphenyl-ethyleneyl group exhibited twisted propeller conformations, whose torsion angle had reached to 75.03°, 60.51,° and 46.35°, respectively. Such distorted structure

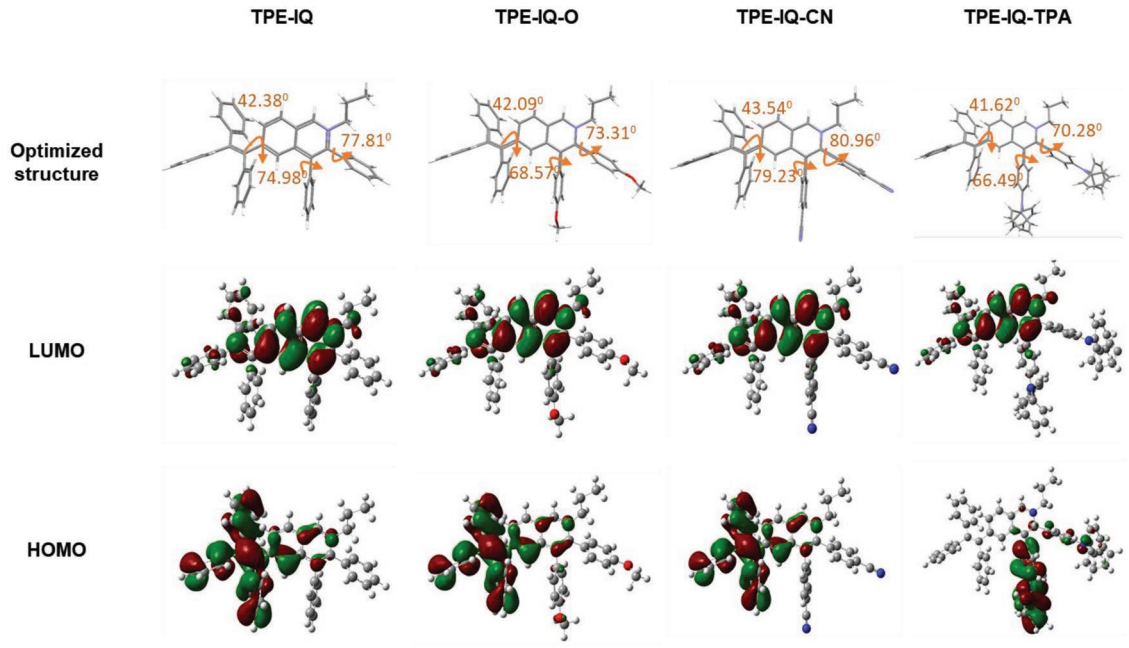

Figure 1. Optimized structures and frontier molecular orbitals for TPE-IQ, TPE-IQ-O, TPE-IQ-CN, and TPE-IQ-TPA removing the counter anion. Calculations were performed by density functional theory calculations at the B3LYP/6-31G* level using the Gaussian 09 program. Hydrogen, carbon, nitrogen, and oxygen were shown in white, gray, blue, and red, respectively. The dihedral angles from isoquinolinium plane of each phenyl groups were noted nearby.

and the large distances between the nearest two isoquinolinium planes demonstrated there was no detrimental π–π interactions in the crystals, which would be effective suppression of aggregation-caused fluorescence quenching. Meanwhile, some multiple weak intermolecular interactions in lattice were observed, such as C—H$\cdots\pi$ interaction, which contributed to restricting intramolecular motion in crystal.

2.2. Theoretical Calculations

To further understand the structural modification orientated effect on photophysical properties of these TPE-IQ-based AIEgens, the density functional theory calculations were performed at the basis set of B3LYP/6-31G* via Gaussian 09. As shown in Figure 1, the optimized structures of the four TPE-IQ-based AIEgens had similar torsion angles between triphenylethyleneyl group and isoquinolinium salt plane about 40°, and almost propeller conformations of triphenyl-ethyleneyl group were observed among them, which is similar to what is observed in the crystal of TPE-IQ-TPA. Interestingly, the two phenyl group originating from diphenyl acetylene derivatives on isoquinolinium ring had larger torsion angles of about 80°, which would lead to a larger spatial structure for suppressing detrimental π–π stacking. Meantime, TPA group in TPE-IQ-TPA exhibited the twisted conformation as that of its crystal structure, implying this calculation results are basically reliable (Figure 1).

As is expected, the lowest unoccupied molecular orbitals (LUMOs) mainly located at the isoquinolinium core due to its stronger electron-withdrawing ability of cation species. However, their highest occupied molecular orbitals (HOMOs) showed obvious difference. For TPE-IQ, TPE-IQ-O, and TPE-IQ-CN, the HOMOs predominantly centered on triphenylethylene, indicating they would have the similar optical behaviors. While for TPE-IQ-TPA, due to stronger electron-donating capability of TPA, the electron cloud of HOMO was transferred to the triphenylamine part, implying its intramolecular charge transfer (CT) process was different from the other three molecules above. Luckily, the HOMOs of these TPE-IQ-based AIEgens were all mainly localized on typical restriction of intramolecular rotation (RIR) blocks (triphenylethylene or triphenylamine), so their AIE features were expected according to previous reports.[21,22]

2.3. Photophysical Properties

As shown in **Figure 2**A and **Table 1**, the absorption maximas of TPE-IQ-CN, TPE-IQ, and TPE-IQ-O in dimethyl sulfoxide (DMSO) solutions are nearly identical at 396, 391, and 382, respectively, which are consistent with their extremely similar distributions of HOMO and LUMO of them in calculation above. When attaching some groups with different electron effect to the electron-deficient isoquinolinium core, their derivatives showed little difference in CT state absorption located at about 400 nm (Figure 2A), which could be attributed to their different CT ability. The introduction of cyanogen group significantly increased the electron-deficiency of isoquinolinium salt so that the D-A effect was strengthened when triphenylethylene group was considered as a donor, whose emission peak in film had an obvious redshite to 559 than 543 nm for TPE-IQ and 540 nm for TPE-IQ-O (Figure 2B). While for TPE-IQ-TPA, its absorption and fluorescence spectra were different from the

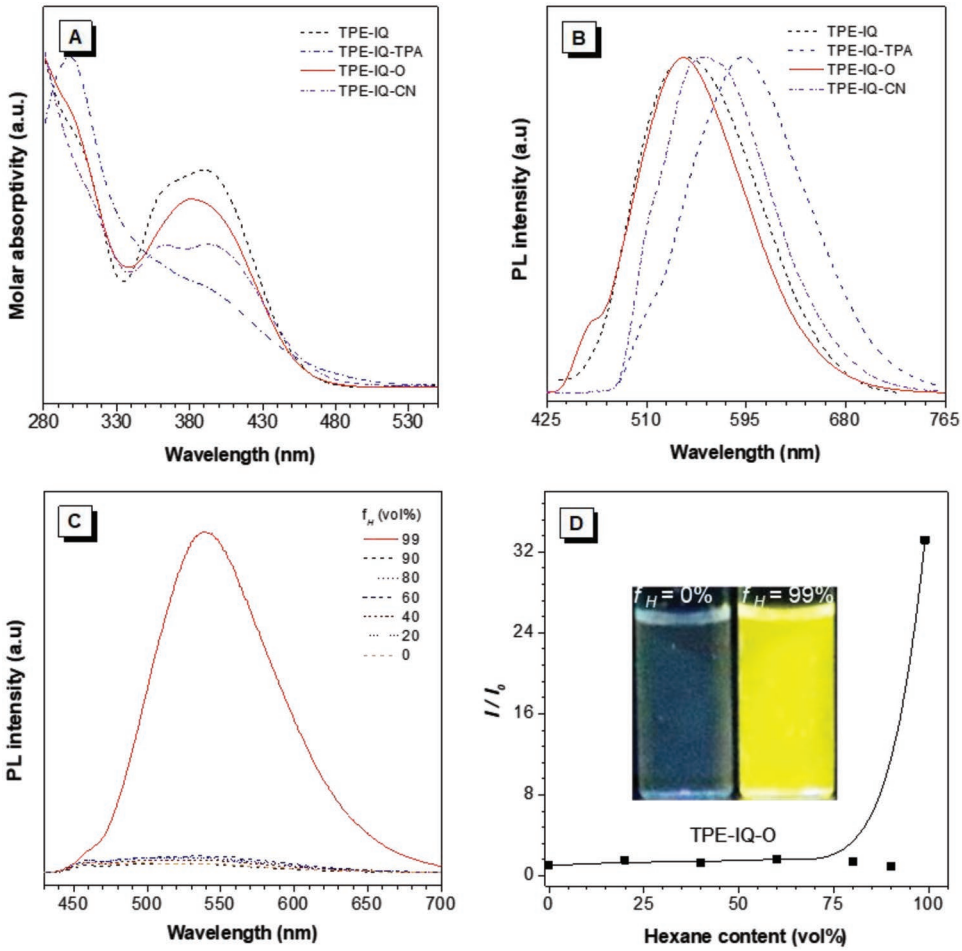

Figure 2. A) UV–vis spectrum of TPE-IQ-CN, TPE-IQ, TPE-IQ-O, and TPE-IQ-TPA in DMSO solution (10^{-5} M). B) TPE-IQ-CN, TPE-IQ, TPE-IQ-O, and TPE-IQ-TPA in solid states and the excitation wavelengths are 392, 390, 382, and 400 nm, respectively. C) Photoluminescence (PL) spectra of TPE-IQ-O in THF/hexane mixtures with different hexane fractions (f_H) under the same excitation conditions. D) I/I_0 plots of TPE-IQ-O in a mixture of hexane-THF, where I is represented as intensity with different hexane volume fractions (f_H), and I_0 is initial intensity in THF. Inset: fluorescent photos of THF/hexane mixtures of TPE-IQ-O at $f_H = 0$ and 99 vol% taken under 365 nm UV illumination from a hand-held UV lamp. Concentration: 10×10^{-6} M.

three compounds above and its emission peak in film was at 592 nm, which might be attributed to its different electronic transition process as calculation described.

For discussing whether these compounds inherited the AIE feature from TPE-IQ,[19] their photoluminescence (PL) spectra were measured in the solution and aggregate states as evidence (Figure 2C,D). Using TPE-IQ-O as an example, TPE-IQ-O emitted weakly in pure tetrahydrofuran (THF) solution. Its emission remained low even when a large amount of hexane (95 vol%) was added to the THF solution. However, further increasing the hexane fraction to 99 vol%, where a threshold of solubility was reached, TPE-IQ-O aggregates were formed and a strong emission peak at 539 nm was detected and bright yellow fluorescence was observed under 365 nm UV illumination (Figure 2D), demonstrating its AIE characteristics. And the similar process could be observed in TPE-IQ-CN and

Table 1. Photophysical properties of TPE-IQ-CN, TPE-IQ, TPE-IQ-O, and TPE-IQ-TPA.

AIEgens	λ_{abs}[a] [nm]	λ_{em}[b] [nm]	Φ_F [%]		τ [ns]		k_r [10^7 s^{-1}][d]		k_{nr} [10^7 s^{-1}][e]	
			Soln[c]	Film	Soln[c]	Film	Soln	Film	Soln	Film
TPE-IQ	390	543	2.3	8.5	4.56	1.63	0.5	5.2	1.7	0.9
TPE-IQ-O	382	540	1.6	7.2	6.64	1.96	0.2	3.7	1.3	1.4
TPE-IQ-CN	392	559	1.7	6.8	5.25	1.51	0.3	4.5	1.6	2.1
TPE-IQ-TPA	298/380	592	1.7	7.4	7.23	4.92	0.2	1.5	1.2	0.5

[a]Measured in DMSO solutions; [b]Film; [c]Measured in THF solutions; [d]k_r = radiative decay rate (Φ_F/τ); [e]k_{nr} = nonradiative decay rate ($1/\tau - k_r$).

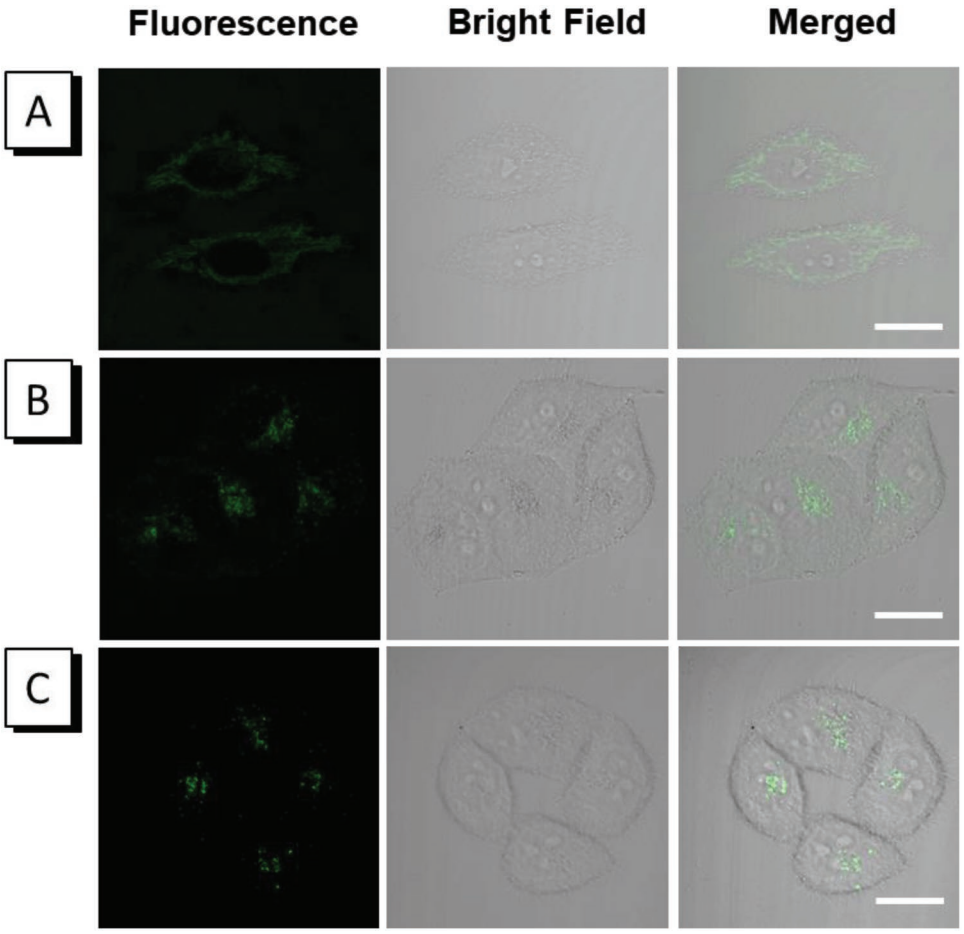

Figure 3. CLSM images of HeLa cells stained with A)TPE-IQ-O (1×10^{-6} M, 15 min), B)TPE-IQ-CN (2×10^{-6} M, 2.5 h), and C)TPE-IQ-TPA (2×10^{-6} M, 2.5 h) and bright field images of HeLa cells stained with TPE-IQ-O, TPE-IQ-CN, and TPE-IQ-TPA. Scale bar = 20 μm.

TPE-IQ-TPA, implying the change of substitutes and HOMOs distribution has no effect on their AIE behaviors.

At the same time, the quantum yield (QY) and lifetime were measured in pure THF and in the solid state for a comprehensive investigation. These compounds were faintly emissive in THF solutions with quantum yield ($\Phi_{F,\ soln.}$) of 1.6–2.3 (%), which were enhanced in the solid powders with $\Phi_{F,\ solid}$ of 11.4–16.2 (%). Clearly, the PL and QY measurements demonstrated that these compounds exhibit the AIE property as shown in Figure 2C and Table 1. Furthermore, the radiative decay rate (K_r) and nonradiative decay rate (K_{nr}) of these TPE-IQ-based compounds in the solution and films were calculated, and their AIE activities originated from the synergistic effect of the increment of K_r and the decrement of K_{nr}, indicating their vibration and rotation had been suppressed in aggregates following restriction of intramolecular motion mechanism (RIM).[23]

2.4. Cell Imaging

Inspired by that TPE-IQ is reported to be a mitochondrion-targeting AIEgen, we expect these TPE-IQ-based AIEgens can inherit some selectivity to specific organelles owing to their cationic structures. So, HeLa cells were used as a cell model, and the bioimaging property of TPE-IQ-O in HeLa cells was first investigated using a confocal laser scanning microscopy (CLSM). The accumulation of this dye molecule was probably highly concentrated in certain organelles and the aggregates of TPE-IQ-O in these organelles were found to increase with different incubation time (Figure S10, Supporting Information). After different incubation concentrations (0.1, 0.5, and 1×10^{-6} M) in live Hela cells for a short incubation time (15 min), bright fluorescence of TPE-IQ-O from the filamentous structures in cytoplasm could be collected (Figure S11, Supporting Information), which is the typical morphology of mitochondria[11] and the costained experiment with MitoTracker Red CMCRos (MTR), a commercially available mitochondrial imaging agent, also confirmed that (**Figure 4**). As shown in Figure 4A, the images stained with TPE-IQ-O were well overlapped with those labeled with MTR with Pearson's correlation coefficient of 0.93, demonstrating that TPE-IQ-O can target mitochondria in high specificity. Interestingly, such phenomenon cannot be found for TPE-IQ-CN and TPE-IQ-TPA in the same incubation conditions. By contrast, the bright fluorescence of these two molecules could be clearly shown in the cytomembrane which was like not to enter cells even prolonging the time to 60 min (Figure S12, Supporting Information). However, when extending the incubation time to 2.5 h, we could find the bright

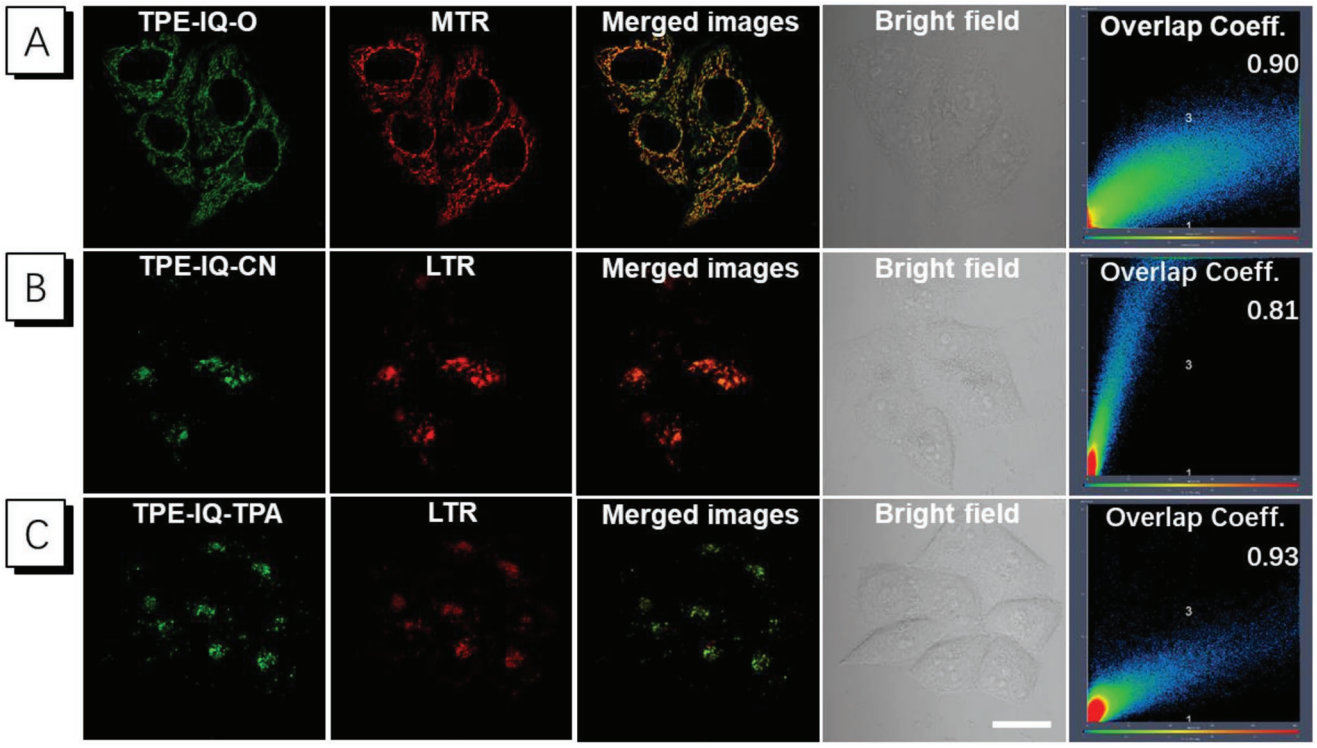

Figure 4. Colocalization images of HeLa cells stained with A) 1×10^{-6} M TPE-IQ-O, B) 2×10^{-6} M TPE-IQ-CN, C) 2×10^{-6} M TPE-IQ-TPA and MTR (100×10^{-9} M) or LTR (1×10^{-6} M). All the images share the same scale bar; scale bar: 20 µm.

fluorescence was all inside the cells (**Figure 3**), and from the aggregation position of the fluorescence, we can infer these two dyes can target lysosome. Hence, HeLa cells were used to be costained with these two compounds and commercial lysosome-targeting dye LysoTracker Red DND-99 (LTR). At different excitation wavelengths, red fluorescence from LTR and green fluorescence from TPE-IQ-CN and TPE-IQ-TPA were readily observed (Figure 4B,C). The lysosome colocation correlation coefficient is more than 80%, suggesting that TPE-IQ-CN and TPE-IQ-TPA can specifically target the lysosome.

2.5. Mechanism of Different Organelles-Targeting

Why are structurally similar compounds with different organelle staining? Referred to the literature reported before,[25] it is essential to understand the structural character of the targets. For mitochondrion, it has a very large membrane potential up to −180 mV, which is more negative than that of other cellular components.[24] For lysosome, it is a spherical vesicle containing hydrolytic enzymes with an acid environment (pH = 4.7).[11,25] Many foreign substances need to be encapsulated in lysosomes to be utilized by cells, which is a way of cell self-protection. They degrade extracellular material that has been internalized by endocytosis and intracellular components that have been sequestered by autophagy.[26]

Taking all described above into consideration, combining with the time these compounds entering cells cost, studies on the way of cellular uptake for further discussing the mechanism by which they selectively image mitochondria (for TPE-IQ-O) or lysosomes (for TPE-IQ-CN and TPE-IQ-TPA) were elaborated clearly. For TPE-IQ-O, blockage of cellular uptake was observed when HeLa cells was incubated at 4 and 37 °C or pretreated with kinds of inhibitors of endocytosis (NH_4Cl, Chloroquine, Dynasore and Cytochalasin D). As shown in **Figures 5**A and **6**, a passive pathway and a nonendocytotic mechanism for TPE-IQ-O was demonstrated due to its temperature-independence and inhibitors of endocytosis having no effect on penetrating to the membrane. So, TPE-IQ-O could target mitochondrion owing to its cationic species. To further confirm that TPE-IQ-O targeting behavior originates from electrostatic interaction, we fixed the cells with paraformaldehyde to destroy the mitochondrial membrane potential (MMP), and found that the molecules were unable to stain mitochondria (Figure S19, Supporting Information). This indicates that TPE-IQ-O bonded to the mitochondrial membrane not by covalent bonds but by electrostatic interaction.

By contrast, it was a temperature-dependent passive pathway for TPE-IQ-CN and TPE-IQ-TPA (Figure 5B,C), with which fluorescence could be clearly observed in HeLa cells treated under the condition of 37 °C for 3 h but no fluorescence in 4 °C. To confirm the internalization mechanism of TPE-IQ-CN and TPE-IQ-TPA in HeLa cells, an endocytosis inhibition experiment was employed. We could find there was no fluorescence in the cells after incubating HeLa cells with Cytochalasin D for TPE-IQ-TPA (Figure 6), while the fluorescence nearly all aggregated in the cytomembrane without entering the cells for TPE-IQ-CN (Figure 6), indicating that endocytosis is the transport mechanism for internalization of TPE-IQ-CN and TPE-IQ-TPA. According to the time-dependent and temperature-independent internalization process in HeLa, it is reasonable that TPE-IQ-CN

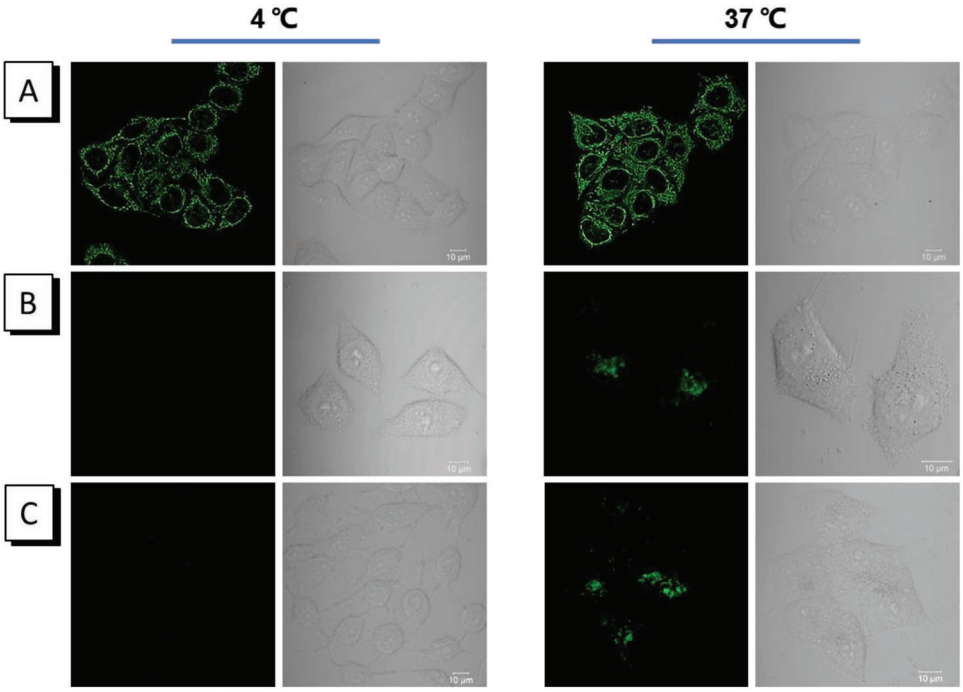

Figure 5. Fluorescent and bright field images of HeLa cells stained with A)TPE-IQ-O (1×10^{-6} M, 10 min), B)TPE-IQ-CN (1×10^{-6} M, 2.5 h), and C)TPE-IQ-TPA (1×10^{-6} M, 2.5 h) at different temperature 4 and 37 °C. Scale bar = 10 μm.

and TPE-IQ-TPA pass through the cell membrane via endocytosis and localize in lysosomes.[25] Namely, TPE-IQ-CN and TPE-IQ-TPA entered cells by endocytosis as foreign matters, which will get to the lysosome when entering cells.[27] But even after incubating HeLa cells with TPE-IQ-CN and TPE-IQ-TPA for 48 h, fluorescence located in lysosome was still observed, which was confirmed by the costained experiment (Figure S18, Supporting Information). So, TPE-IQ-CN and TPE-IQ-TPA can be considered as lysosome-targeting dyes.

According to the high lipophilicity and low charge density favoring cellular uptake described by the Nernst equation,[28] the charge density and size of these molecules can be regarded as important points to account for their different ways of cellular uptake. The nanoparticle size from dynamic light scattering (DLS) measurement and zeta potential clearly assessed this relationship as shown in **Figure 7**. Notably, the size distributions of these compounds were 164.0 nm for TPE-IQ-O, 92.9 nm for TPE-IQ-CN and 144.6 nm for TPE-IQ-TPA, respectively, while their zeta potential showed great difference. Herein, the observed difference of cellular uptake can be attributed to the high-energy barrier between these TPE-IQ-based AIEgens and cell membrane. Namely TPE-IQ-CN and TPE-IQ-TPA with small diameter and high zeta potential of 19.6 and 33.1 mV have high energy barrier between hydrophobic membrane and probe, resulting in membrane impermeability.[29]

2.6. Cytotoxicity

The cytotoxicity of these compounds toward both Hela cells was assayed with the standard MTT method. As shown in **Figure 8**, the viability of Hela cells was measured to be only 31% after treatment with 10×10^{-6} M TPE-IQ-O for 24 h, while the viability, treated with TPE-IQ-CN and TPE-IQ-TPA under the same condition, was over 80%. Why do these compounds show great difference in the respect of cytotoxicity? As referred to above, TPE-IQ-O, TPE-IQ-CN, and TPE-IQ-TPA are cationic compounds, TPE-IQ-O specially target to the mitochondrial and we speculate that the binding of such molecules to mitochondria changes the MMP, making it toxic to cells. To prove this inference, MMP was measured with a commercial JC-1 dye on the basis i) it shows red fluorescence upon aggregation in healthy negatively charged mitochondria, and ii) it becomes green emissive when mitochondrial membrane($\Delta\psi_m$) is reduced and mitochondria is damaged.[30] So, we use JC-1 dye as an indicator to discern whether TPE-IQ-O destroys membrane of mitochondrial. As can be seen from **Figure 9**, red fluorescence was observed for polarized mitochondria and nearly no green fluorescence was observed for polarized mitochondria in Hela cells without treatment. However, after incubation with TPE-IQ-O for 60 min, the red fluorescence became weak, and the green fluorescence emerged simultaneously. And after incubation with TPE-IQ-O for 100 min, the green fluorescence further enhanced and the morphology of mitochondrial changed a lot, indicating the reduction of $\Delta\psi_m$. By contrast, the similar phenomenon was not observed for TPE-IQ-CN and TPE-IQ-TPA. These results hint that the cytotoxicity of TPE-IQ-O toward Hela cells is caused by damaged membrane of mitochondria.[31]

2.7. ROS and PDT

The efficiency of ROS generation is of great importance for PDT,[32] and thus the ability of ROS generation for TPE-IQ-based AIEgens upon white light irradiation was evaluated. Analyzing ROS

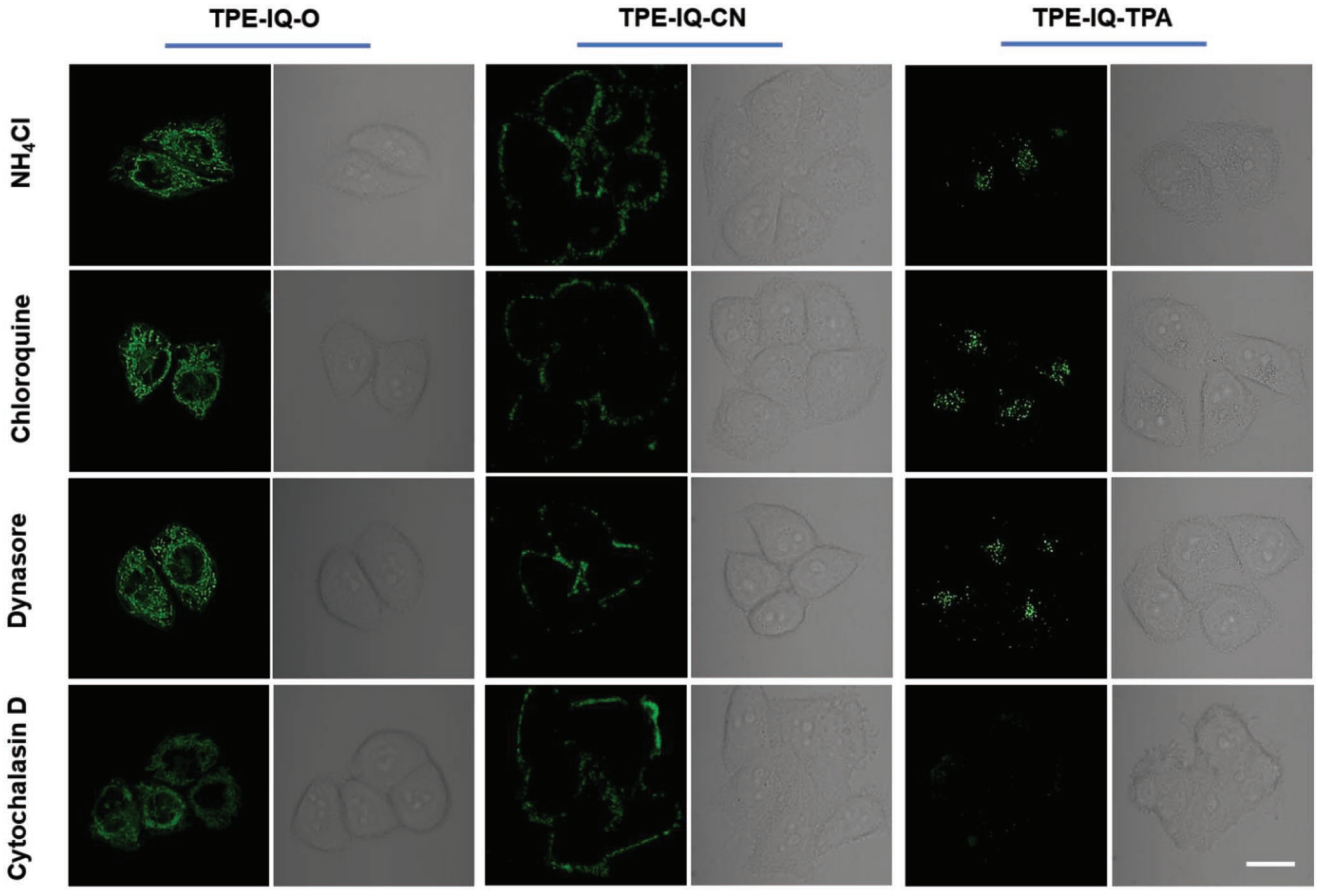

Figure 6. The fluorescent and bright field images of HeLa cells pretreated with endocytic inhibitors NH_4Cl (50×10^{-3} M), chloroquine (50×10^{-6} M), Dynasore (40×10^{-6} M) and Cytochalasin D (5×10^{-6} M), respectively and then incubated with 1×10^{-6} M TPE-IQ-O at 37 °C for 30 min, 2×10^{-6} M TPE-IQ-CN at 37 °C for 3 h and 2×10^{-6} M TPE-IQ-TPA at 37 °C for 3 h . Scale bar = 20 μm.

generation efficiency (**Figure 10**A), we could find in the presence of TPE-IQ-based AIEgens, the emission intensity of 2,7-dichlorodihydrofluorescein (DCFH), served as an indicator and exhibited the "turn-on" fluorescent signal activated by ROS,[33] gradually enhanced over 20-fold to 45-fold with the increase of irradiation time by white light, whereas that of TPE-IQ-based AIEgens or DCFH alone were still weak. The increasing rate of the relative emission intensity with the increase of irradiation time, revealing the overall quantity of ROS generation by AIEgens, showed difference after irradiated for 2 min due to their different single-triplet energy gap of these TPE-IQ-based AIEgens.

To make clear whether the ROS production of these TPE-IQ-based AIEgens as photosensitizers also suits for killing cancer cells, their phototoxicity of TPE-IQ-CN, TPE-IQ-O, and TPE-IQ-TPA was further evaluated by the method of MTT assay after LED white light irradiation(400–800 nm) for

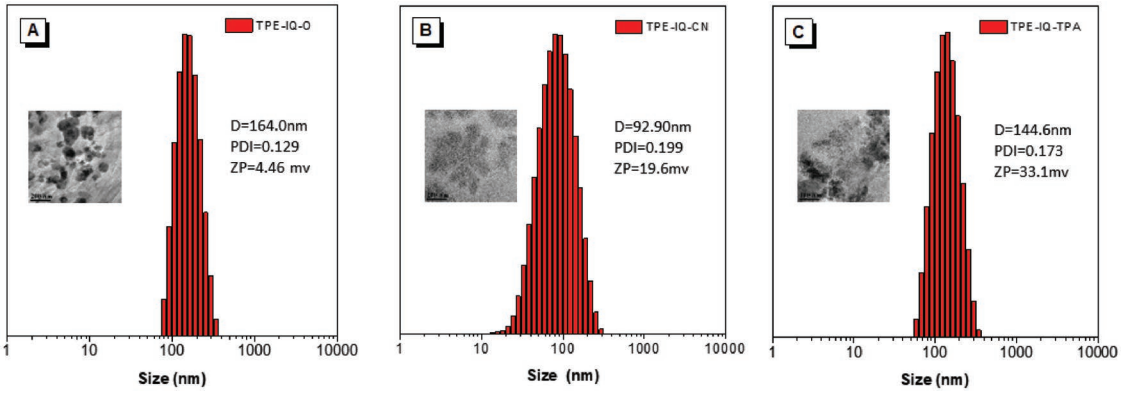

Figure 7. A–C) Size and Zeta Potential (ZP) analysis of TPE-IQ-based AIEgens (10×10^{-6} M) in the aqueous solution.

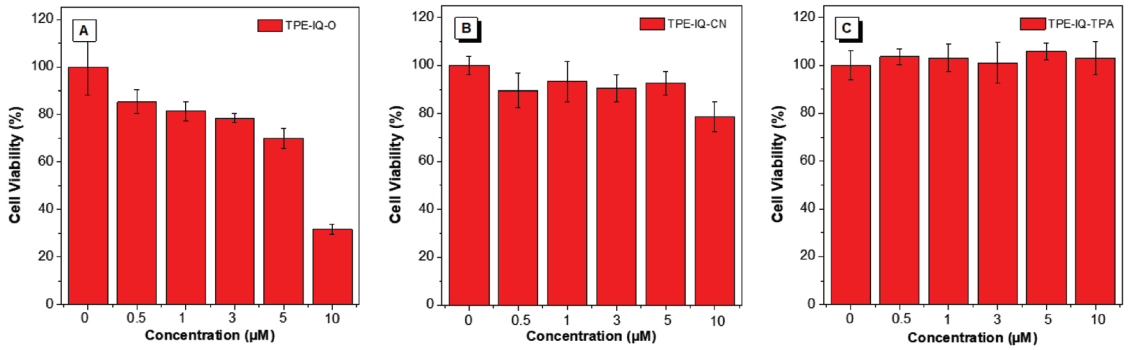

Figure 8. A–C) Dark cytotoxicity assessment of TPE-IQ-based AIEgens on Hela cells determined by MTT assay.

30 min (Figure 10B–D),[34] whereas that in dark as the control. Although MTT assay in dark had some experimental errors from the cellular stress effect and interference of probes taking up by cells, the overall results showed no obvious inhibitory phenomenon in the growth of HeLa cells even in culture medium with high concentration (10×10^{-6} M) treatment except for TPE-IQ-O. Accordingly, under a general LED white light irradiation, the distinct cytotoxicity of AIEgens was observed for TPE-IQ-O (3×10^{-6} M) with the viability of Hela cells being below 20% (Figure 10B). Due to the work concentration being 1×10^{-6} M, TPE-IQ-O still could be regarded as a photosensitizer for solid tumor photodynamic therapy. By contrast, the viability of Hela cells treated with TPE-IQ-CN (10×10^{-6} M) and TPE-IQ-TPA (10×10^{-6} M) was measured to be 51% and 43%, respectively, under the same white light irradiation condition, of which the photodynamic therapy effect in HeLa cells was inferior to that of TPE-IQ-O. This phenomenon may be attributed to the ability of ROS generation and the different targets of these TPE-IQ-based AIEgens. That is to say, the photodynamic therapy effect of photosensitizer targeting lysosome is not as good as that of photosensitizer targeting mitochondrial.

3. Conclusion

In summary, a series of new TPE-IQ-based AIEgens were prepared via attaching different groups with electron and steric-hindrance effect to the electron-deficient isoquinolinium core, and they all exhibited AIE characteristics with different emission colors and Zeta potentials when aggregated as nanoparticles. In addition, TPE-IQ-O could specially target mitochondria as our reported TPE-IQ, while TPE-IQ-CN and TPE-IQ-TPA showed good target to lysosome. Employing detailed and systematic experiments, the way of cellular uptake caused by different energy barrier between these TPE-IQ-based AIEgens and cell membrane was confirmed, revealing the relationship between electrostaticity and targeting organelles. Thanks for the efficient ROS generation of these TPE-IQ-based AIEgens

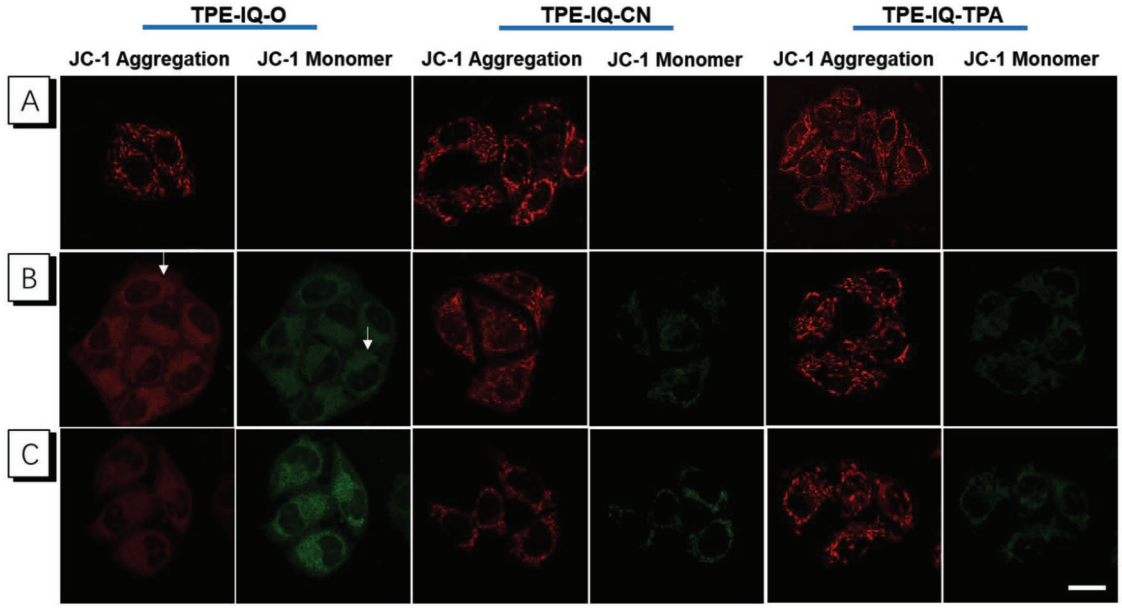

Figure 9. Monitoring mitochondrial membrane potential ($\Delta\psi_m$) of Hela cells using mitochondrial membrane potential commercial dye JC-1 following treated with TPE-IQ-O (5×10^{-6} M), TPE-IQ-CN (5×10^{-6} M), and TPE-IQ-TPA (5×10^{-6} M) on different time points A) 0 min, B) 60 min, and C) 180 min. White arrow represents the changed mitochondrial morphology. Scale bar = 20 μm.

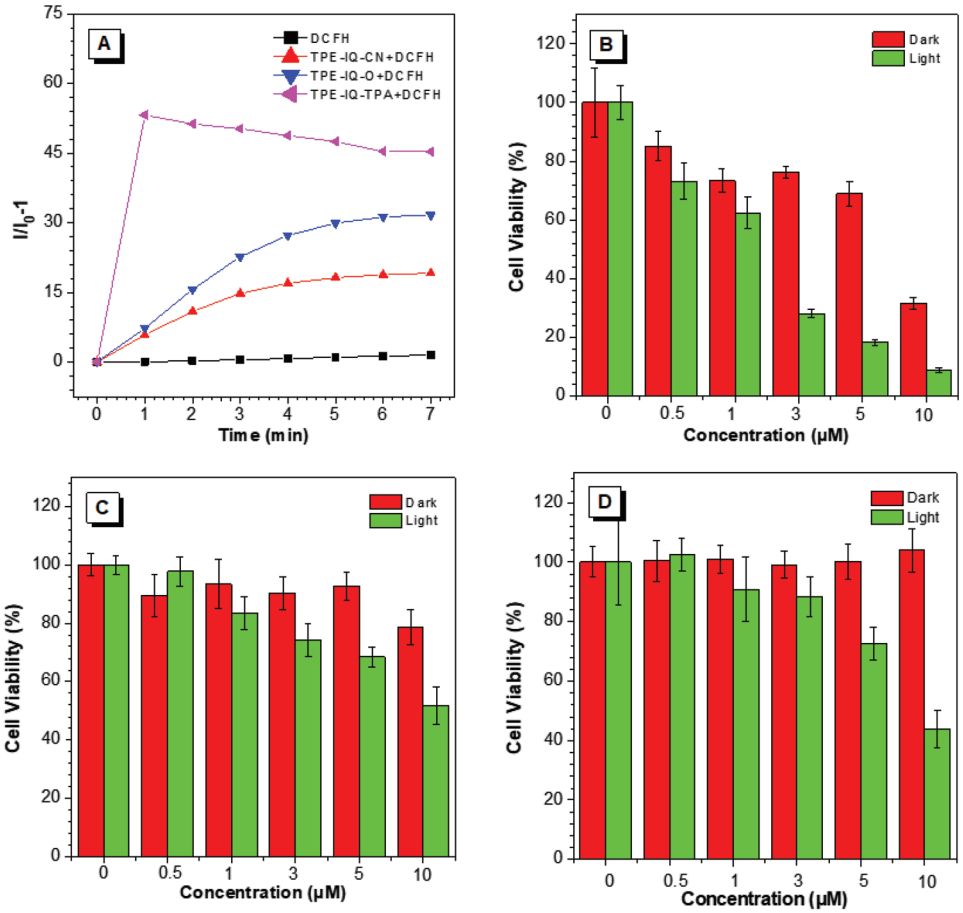

Figure 10. A) Relative change in fluorescence intensity (I/I_0–1) at 525 nm of DCFH, TPE-IQ-based AIEgens (TPE-IQ-CN, TPE-IQ-O, and TPE-IQ-TPA), mixtures of DCFH and TPE-IQ-based AIEgens in PBS upon white light irradiation for different times. Concentrations: 10×10^{-6} M for TPE-IQ-based AIEgens and 1×10^{-6} M for DCFH. B–D) Cytotoxicity of HeLa cells stained with different concentrations of B) TPE-IQ-O, C) TPE-IQ-CN, and D) TPE-IQ-TPA determined by MTT assay in dark and under white light irradiation for 30 min, respectively. Light power: 30 mW cm^{-2}.

under light, they could be use as photosensitizers for PDT. All these intriguing results indicate such readily accessible TPE-IQ-based AIEgens provide a new strategy for construction of functional materials in practical applications.

4. Experimental Section

Materials, instrumentation, and detailed experimental procedures can be found in the Supporting Information.

CCDC 1 904 591 contain the crystallographic data for this paper (Supporting Information). These data can be obtained free of charge from The Cambridge Crystallographic Data Centre via www.ccdc.cam.ac.uk/data_request/cif.

Supporting Information

Supporting Information is available from the Wiley Online Library or from the author.

Acknowledgements

K.C. and R.Z. contributed equally to this work. This work was financially supported by National Natural Science Foundation of China (Nos. 21788102, 51673118, 81472401, 81772708, and 21975077), Science & Technology Program of Guangzhou (No. 201804010218), the Innovation and Technology Commission of Hong Kong (No. ITC-CNERC14SC01), the Fundamental Research Funds for the Central Universities (No. D2190960), and Fund of Key Laboratory of Luminescence from Molecular Aggregates of Guangdong Province (2019B030301003).

Conflict of Interest

The authors declare no conflict of interest.

Keywords

aggregation-induced emission, isoquinolinium derivatives, mitochondria and lysosome targeting, reactive oxygen species (ROS), structure–properties relationship

Received: August 22, 2019
Revised: September 25, 2019
Published online: November 13, 2019

[1] a) R. W. Sinkeldam, N. J. Greco, Y. Tor, *Chem. Rev.* **2010**, *110*, 2579; b) C. Zhang, J. Lin, *Chem. Soc. Rev.* **2012**, *41*, 7938; c) X. Li, M. Rui, J. Song, Z. Shen, H. Zeng, *Adv. Funct. Mater.* **2015**, *25*, 4929.

[2] a) M. J. Rust, M. Bates, X. Zhuang, *Nat. Methods* **2006**, *3*, 793; b) F. Peng, Y. Su, Y. Zhong, C. Fan, S. T. Lee, Y. He, *Acc. Chem. Res.* **2014**, *47*, 612; c) L. Yan, Y. Zhang, B. Xu, W. Tian, *Nanoscale* **2016**, *8*, 2471.
[3] a) Y. H. M. Chan, W. F. Marshall, *Science* **2012**, *337*, 1186; b) H. Zhu, J. Fan, J. Du, X. Peng, *Acc. Chem. Res.* **2016**, *49*, 2115. c) F. Wu, X. Wu, Z. Duan, Y. Huang, X. Lou, F. Xia, *Small* **2019**, *15*, 1804839.
[4] a) D. C. Wallace, *Nat. Rev. Cancer* **2012**, *12*, 685; b) X. Song, N. Li, C. Wang, Y. Xiao, *J. Mater. Chem. B* **2017**, *5*, 360.
[5] a) J. Zielonka, J. Joseph, A. Sikora, M. Hardy, O. Ouari, J. Vasquez-Vivar, B. Kalyanaraman, *Chem. Rev.* **2017**, *117*, 10043; b) Y. Cheng, J. Dai, C. Sun, R. Liu, T. Zhai, X. Lou, F. Xia, *Angew. Chem., Int. Ed.* **2018**, *57*, 3123.
[6] a) F. Xue, P. Wei, X. Ge, Y. Zhong, C. Cao, D. Yu, T. Yi, *Dyes Pigm.* **2018**, *156*, 285; b) B. A. Davies, J. R. Lee, A. J. Oestreich, D. J. Katzmann, *Chem. Rev.* **2009**, *109*, 1575.
[7] a) X. Ma, N. Gong, L. Zhong, J. Sun, X. J. Liang, *Biomaterials* **2016**, *97*, 10; b) M. Jeyakumar, R. A. Dwek, T. D. Butters, F. M. Platt, *Nat. Rev. Neurosci.* **2005**, *6*, 713.
[8] a) W. Z. Yuan, P. Lu, S. Chen, J. W. Lam, Z. Wang, Y. Liu, S. H. Kwok, Y. Ma, B. Z. Tang, *Adv. Mater.* **2010**, *22*, 2159; b) Y. Wang, Y. Chen, H. Wang, Y Cheng, X. Zhao, *Anal. Chem.* **2015**, *87*, 5046.
[9] a) C. W. T. Leung, Y. Hong, S. Chen, E. Zhao, J. W. Y. Lam, B. Z. Tang, *J. Am. Chem. Soc.* **2013**, *135*, 62; b) N. C. Shaner, P. A. Steinbach, R. Y. Tsien, *Nat. Methods* **2005**, *2*, 905. c) K. C. Chong, F. Hu, B. Liu, *Mater. Chem. Front.* **2019**, *3*, 12.
[10] a) J. Mei, N. L. Leung, R. T. Kwok, J. W. Lam, B. Z. Tang, *Chem. Rev.* **2015**, *115*, 11718; b) R. T. Kwok, C. W. Leung, J. W. Lam, B. Z. Tang, *Chem. Soc. Rev.* **2015**, *44*, 4228; c) Y. Hong, J. W. Lam, B. Z. Tang, *Chem. Soc. Rev.* **2011**, *40*, 5361; d) Q. Qi, C. Li, X. Liu, S. Jiang, Z. Xu, R. Lee, M. Zhu, B. Xu, W. Tian, *J. Am. Chem. Soc.* **2017**, *139*, 16036.
[11] a) A. Shao, Y. Xie, S. Zhu, Z. Guo, S. Zhu, J. Guo, P. Shi, T. D. James, H. Tian, W. H. Zhu, *Angew. Chem., Int. Ed.* **2015**, *54*, 7275; b) G. Feng, B. Liu, *Acc. Chem. Res.* **2018**, *51*, 1404.
[12] a) Y. Li, Y. Wu, J. Chang, M. Chen, R. Liu, F. Li, *Chem. Commun.* **2013**, *49*, 11335; b) Y. Cheng, C. Sun, X. Ou, B. Liu, X. Lou, F. Xia, *Chem. Sci.* **2017**, *8*, 4571.
[13] a) S. D. Wiedner, L. N. Anderson, N. C. Sadler, W. B. Chrisler, V. K. Kodali, R. D. Smith, A. T. Wright, *Angew. Chem., Int. Ed.* **2014**, *53*, 2919; b) P. Y. Yang, K. Liu, C. Zhang, G. Y. Chen, Y. Shen, M. H. Ngai, S. Q. Yao, *Chem. - Asian J.* **2011**, *6*, 2762.
[14] a) R. Igarashi, Y. Yoshinari, H. Yokota, T. Sugi, F. Sugihara, K. Ikeda, Y. Harada, *Nano Lett.* **2012**, *12*, 5726; b) W. W. W. Hsiao, Y. Y. Hui, P. C. Tsai, H. C. Chang, *Acc. Chem. Res.* **2016**, *49*, 400.
[15] a) E. Ju, Z. Li, Z. Liu, J. Ren, X. Qu, *ACS Appl. Mater. Interfaces* **2014**, *6*, 4364; b) A. Chevalier, Y. Zhang, O. M. Khdour, J. B. Kaye, S. M. Hecht, *J. Am. Chem. Soc.* **2016**, *138*, 12009.
[16] a) J. P. Celli, B. Q. Spring, I. Rizvi, C. L. Evans, K. S. Samkoe, S. Verma, T. Hasan, *Chem. Rev.* **2010**, *110*, 2795; b) F. Hu, S. Xu, B. Liu, *Adv. Mater.* **2018**, *30*, 1801350.
[17] a) C. He, D. Liu, W. Lin, *ACS Nano* **2015**, *9*, 991; b) B. Liu, C. Li, G. Chen, B. Liu, X. Deng, Y. Wei, J. Lin, *Adv. Sci.* **2017**, *4*, 1600540.
[18] a) S. Chakrabortty, B. K. Agrawalla, A. Stumper, N. M. Vegi, S. Fischer, C. Reichardt, S. Rau, *J. Am. Chem. Soc.* **2017**, *139*, 2512; b) G. Feng, W. Qin, Q. Hu, B. Z. Tang, B. Liu, *Adv. Healthcare Mater.* **2015**, *4*, 2667.
[19] E. G. Zhao, H. Q. Deng, S. J. Chen, Y. N. Hong, C. W. T. Leung, J. W. Y. Lam, B. Z. Tang, *Chem. Commun.* **2014**, *50*, 14451.
[20] C. Gui, E. Zhao, R. T. Kwok, A. C. Leung, J. W. Lam, M. Jiang, H. Deng, Y. Cai, W. Zhang, H. Su, B. Z. Tang, *Chem. Sci.* **2017**, *8*, 1822.
[21] M. Jiang, X. Gu, R. T. Kwok, Y. Li, H. H. Sung, X. Zheng, Y. Zhang, J. W. Lam, I. D. Williams, X. Huang, K. S. Wong,, B. Z. Tang. *Adv. Funct. Mater.* **2018**, *28*, 1704589.
[22] L. Pan, Y. Cai, H. Wu, F. Zhou, A. Qin, Z. Wang, B. Z. Tang, *Mater. Chem. Front.* **2018**, *2*, 1310.
[23] J. Chen, C. C. Law, J. W. Lam, Y. Dong, S. M. Lo, I. D. Williams, D. Zhu, B. Z. Tang, *Chem. Mater.* **2003**, *15*, 1535.
[24] N. Kamo, M. Muratsugu, R. Hongoh, Y. Kobatake, *J. Membr. Biol.* **1979**, *49*, 105.
[25] X. J. Chao, K. N. Wang, L. L. Sun, Q. Cao, Z. F. Ke, D. X. Cao, Z. W. Mao, *ACS Appl. Mater. Interfaces* **2018**, *10*, 13264.
[26] P. Saftig, J. Klumperman, *Nat. Rev. Mol. Cell Biol.* **2009**, *10*, 623.
[27] a) X. Chen, Y. Li, S. Li, M. Gao, L Ren, B. Z. Tang, *Adv. Funct. Mater.* **2018**, *28*, 1804362; b) B. Andreiuk, A. Reisch, V. G. Pivovarenko, A. S. Klymchenko, *Mater. Chem. Front.* **2017**, *1*, 2309.
[28] a) J. Zielonka, J. Joseph, A. Sikora, M. Hardy, O. Ouari, J. Vasquez-Vivar, G. Cheng, M. Lopez, B. Kalyanaraman, *Chem. Rev.* **2017**, *117*, 10043; b) D. Wang, H. Su, R. T. K. Kwok, X. Hu, H. Zou, Q. Luo, M. M. S. Lee, W. Xu, J. W. Y. Lam, B. Z. Tang, *Chem. Sci.* **2018**, *9*, 3685.
[29] a) E. L. da Rocha, G. F. Caramori, C. R. Rambo, *Phys. Chem. Chem. Phys.* **2013**, *15*, 2282. b) H. Y. Yin, J. Tang, J. L. Zhang, *Chin. Chem. Lett.* **2018**, *29*, 267.
[30] a) Z. Xue, R. Zhu, S. Wang, J. Li, J. Han, J. Liu, S. Han, *Anal. Chem.* **2018**, *90*, 2954. b) R. A. J. Smith, C. M. Porteous, A. M. Gane, M. P. Murphy, *Proc. Natl. Acad. Sci. USA* **2003**, *100*, 5407.
[31] Y. Huang, G. Zhang, F. Hu, Y. Jin, R. Zhao, D. Zhang, *Chem. Sci.* **2016**, *7*, 7013.
[32] a) N. Alifu, X. Dong, D. Li, X. Sun, A. Zebibula, D. Zhang, G. Zhang, J. Qian, *Mater. Chem. Front.* **2017**, *1*, 1746; b) L. L. Rui, H. L. Cao, Y. D. Xue, L. C. Liu, L. Xu, Y. Gao, W. A. Zhang, *Chin. Chem. Lett.* **2016**, *27*, 1412.
[33] Y. Nosaka, A. Y. Nosaka, *Chem. Rev.* **2017**, *117*, 11302.
[34] Y. Zheng, H. Lu, Z. Jiang, Y. Guan, J. Zou, X. Wang, R. Cheng, H. Gao, *J. Mater. Chem. B* **2017**, *5*, 6277.

